Vortex stabilization by means of spatial solitons in nonlocal media

Citation for published version:
Izdebskaya, Y, Krolikowski, W, Smyth, N & Assanto, G 2016, 'Vortex stabilization by means of spatial solitons in nonlocal media' Journal of Optics, vol. 18, no. 5, 054006. DOI: 10.1088/2040-8978/18/5/054006

Digital Object Identifier (DOI):
10.1088/2040-8978/18/5/054006

Published In:
Journal of Optics

Vortex stabilization by means of spatial solitons in nonlocal media

Yana Izdebskaya,[1] Wieslaw Krolikowski,[2] Noel F. Smyth,[3] and Gaetano Assanto[4]

[1] *Laser Physics Center, Research School of Physics and Engineering, The Australian National University, Canberra ACT 0200, Australia*

[2] *Laser Physics Center, Research School of Physics and Engineering, The Australian National University, Canberra ACT 0200, Australia*
Texas A & M University at Qatar, Doha, Qatar

[3] *School of Mathematics, University of Edinburgh, Edinburgh EH9 3FD, Scotland, U.K.*

[4] *NooEL— Nonlinear Optics and OptoElectronics Lab, University of Rome "Roma Tre", I-00146 Rome, Italy*
Optics Laboratory, Tampere University of Technology, FI-33101 Tampere, Finland

(Dated: February 9, 2016)

Abstract. We investigate how optical vortices, which tend to be azimuthally unstable in nonlinear media, can be stabilized by a copropagating coaxial spatial solitary wave in nonlocal, nonlinear media. We focus on the formation of nonlinear vortex-soliton vector beams in reorientational soft matter, namely nematic liquid crystals, and report on experimental results, as well as numerical simulations.

I. INTRODUCTION

Light beams with optical vortices have attracted growing attention during the past decades[1–4]. Such complex beams are usually associated with a ring-like intensity structure with a zero value at the centre where the electromagnetic field vanishes, and a phase distribution spiralling around it. Besides their rich and intriguing properties, including phase singularities, internal energy circulation and the unique features of their linear and angular momentum distributions, optical vortices offer a wide range of prospective applications in such areas as micro-manipulation[5–9], optical encoding/processing of information[10–14] and sensitivity and resolution enhancement in optical observations and measurements[15,16]. Optical vortex beams can be generated in different types of linear[1–4,17] and nonlinear media[18]. However, they are usually prone to strong dynamical instabilities in self-focusing nonlinear media that tend to amplify local azimuthal modulations of the initial donut shape and split it into fragments which fly away from the initial vortex ring[18].

Nevertheless, as was shown in a few theoretical papers, if the nonlinearity is accompanied by nonlocality, so that the overall nonlinear perturbation in the medium extends far beyond the beam waist in the transverse plane[19], the propagation of an optical vortex can be stabilised. In particular, stable propagation of spatially localized vortices may become possible in highly nonlocal, nonlinear media with a self-focusing response[20,21]. This prediction was confirmed by experimental results on the existence of stable vortex solitons with unit topological charge in thermal nonlinear media[22]. Nonlocal spatial solitons were also found to be able to stably guide and route vortex beams across an interface or around a defect by counteracting the diffraction and instabilities enhanced by such refractive perturbations[23]. An intense vortex and a co-propagating spatial soliton are expected to form a stable vector soliton in a self-focusing nonlocal media[18], in a similar fashion to bright vector solitons with components of different colours[24,25], spiralling solitons with angular momentum[26–29] and multi-hump soliton structures consisting of two (or more) components which mutually self-trap[18,30–32]. As was reported in recent theoretical and numerical studies[33], such two component vector vortex solitons may be stable in nematic liquid crystals (NLCs) due to the strong reorientational nonlinearity of such soft matter[34,35] and the stabilizing character of the resulting nonlinear, nonlocal potential generated by the superposition of both beam components [33,36]. Thus, an important challenge in nonlinear singular optics remains to reveal the physical mechanisms which will allow the experimental observation of stable optical vortices in realistic nonlinear media.

In this Paper, we observe experimentally and describe theoretically the formation of stable two component vector vortex solitons in nematic liquid crystals. These vector solitons appear in the form of two wavelength self-trapped beams with one of the components carrying a phase singularity and being stabilized by its nonlocally enhanced interaction with the other transverse localized beam, a fundamental spatial soliton. We also find that such vector beams can be generated for certain ranges of the soliton excitation, that is the input beam power.

II. SAMPLE AND EXPERIMENTAL RESULTS

For our experiments we used a planar cell realized by polycarbonate slides held parallel to one another and separated by 110 μm across y in order to contain the 6CHBT NLC mixture. The cell structure is sketched in Figs. 1(a,b). The planar interfaces between the polycarbonate and the nematic liquid crystals provide molecular anchoring by means of mechanical rubbing, ensuring that the elongated molecules are orientated with their main axes in the plane (x, z) of the slides, at an angle $\theta_0 = \pi/4$ with the input wavevector $\mathbf{k}$ along the z direction. Two additional 150 μm thick glass slides at the input and output interfaces seal the cell to prevent lens-like effects and avoid light depolarization. The maximum propagation length along the z axis was 1.1 mm from the input to the output facets.

The experimental setup for the generation of two component, two colour vector vortex solitons is shown in Fig. 1(c). One beam component (red) carries the extraordinarily polarized single charge vortex beam generated by a fork-type amplitude diffraction hologram (DH) using a cw laser beam at wavelength $\lambda_{01} = 671nm$ and power P_r. The second (green)

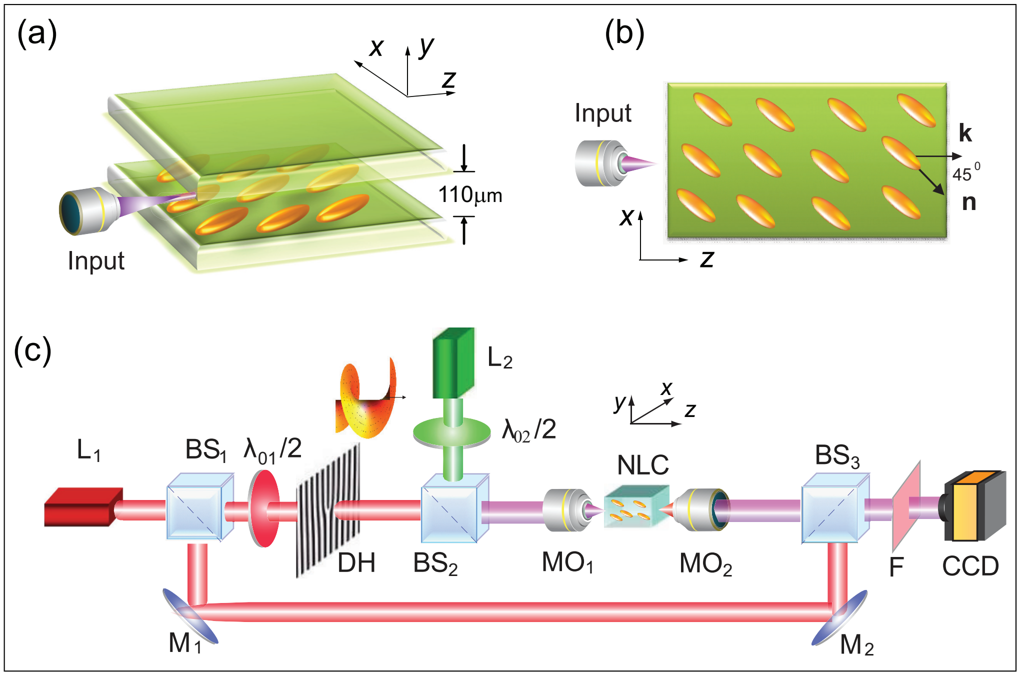

FIG. 1. (Color online) (a) Perspective and (b) top views of the planar cell; the ellipses indicate the oriented molecules; (c) Experimental setup: $L_{1,2}$ are the green ($\lambda_{01} = 671nm$) and red ($\lambda_{02} = 532nm$) cw lasers, $\lambda_0/2$— half wave plates, BS— beam splitters, DH— vortex hologram, M— mirrors, MO_1–10× microscope objective, MO_2–20× microscope objective, NLC— sample, F— filter, CCD— charge-coupled device camera.

component is an extraordinarily polarized fundamental Gaussian beam of wavelength $\lambda_{02} = 532nm$ and power P_g. Figure 2 shows the input beams, with Figs. 2(a,d) showing the corresponding input intensity distributions, Figs. 2(b,e) the schematic phase fronts and Figs. 2(c,f) the intensity profiles of each beam: the green Gaussian beam (left) and the red single charged vortex (right). The two co-polarized beams were injected into the NLC with collinear Poynting vectors along z by a 10× microscope objective (MO_1). The input waists were $w_v \approx 7\mu m$ and $w_g \approx 4\mu m$ for the vortex and fundamental Gaussian beams, respectively. With the half-wave plates $\lambda_{01}/2$ and $\lambda_{02}/2$ we controlled the polarization state of both beams. In order to study the singular phase structure of the vector vortex beams we used a Mach-Zehnder arrangement (beam splitters BS1 and BS3, mirrors M1 and M2). The output light intensity after propagation was monitored by collecting the light at the output using a 20× microscope objective (MO_2) and a high-resolution CCD camera. We monitored the evolution at both wavelengths, but in order to prevent chromatic effects and record the output images of the (red) vortex or green (fundamental) beams separately, we used either red or green filters (F) placed in front of the camera.

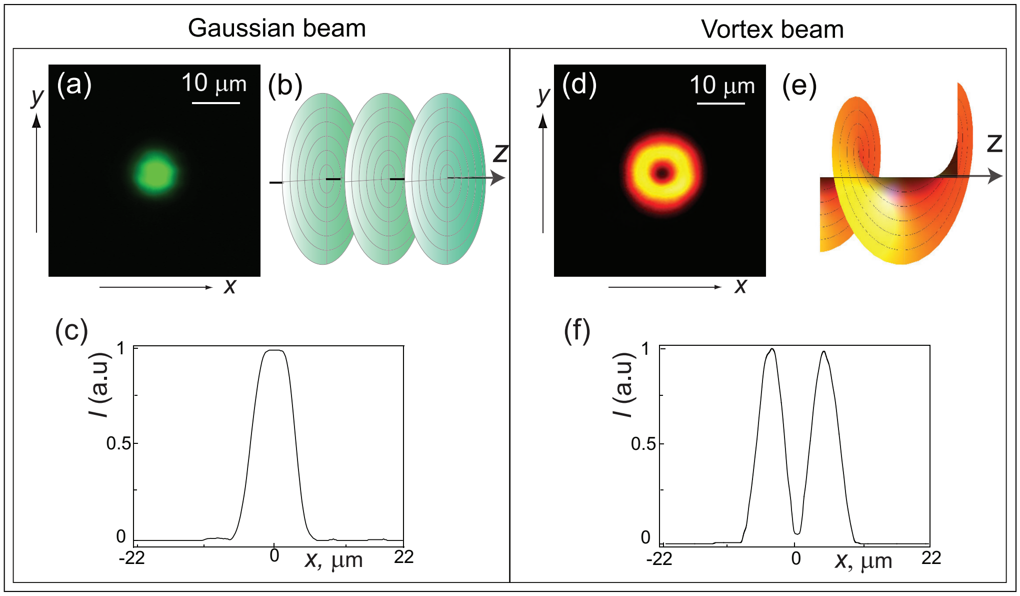

FIG. 2. (Color online) Each vector beam component, i.e. a Gaussian (left) or a single-charge vortex (right) propagating separately in the NLC cell. (a,d) Measured input intensity distributions; (b,e) schematic wavefront views and (c,f) normalized intensity profiles of each beam from the input images (a,d).

We initially investigated the linear and nonlinear behaviour of either component when each beam propagated in the absence of the other. As visible in Figs. 3(a,c), for low input powers of both beams, $P_{g,r} < 0.9\ mW$, the self-focusing is too weak to overcome diffraction. On increasing the power of the green component to $P_g > 2.4\ mW$ the fundamental Gaussian beam undergoes self-focusing and the transverse intensity distribution at the output visibly reduces, so that a spatial soliton is formed, also called a *nematicon* in these materials [see Fig. 3(b)][35]. On the other hand, increasing the input power of the beam which carries angular momentum to $P_r > 5\ mW$ leads to its self-focusing, but such a beam is affected by strong dynamic instabilities which tend to amplify local azimuthal modulations of the initial ring shape and so split the vortex beam into two fragments [Fig. 3(d)][20]. Such a symmetry-breaking azimuthal instability is enhanced by the nonsymmetric configuration of the planar cell and the related anisotropy in the induced refractive index profile. This dynamics is consistent with recently reported results on the astigmatic deformation of a vortex beam in a planar NLC cell and its transformation into a dipole-like transverse intensity distribution[29]. Figures 3(e–h) show the normalized x cross-sections of the intensity profiles in the plane (x, y) for two different powers of both components, as acquired from the output images in Figs. 3(a–d).

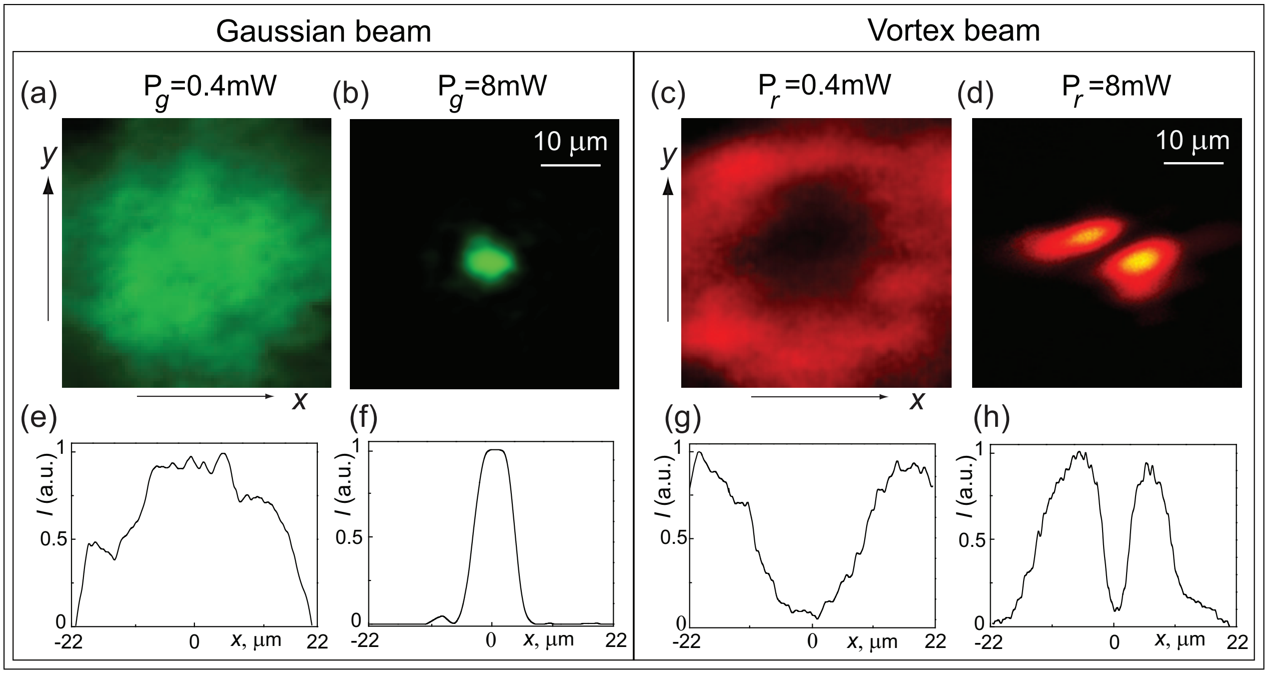

FIG. 3. (Color online) Measured output intensity distributions (a–d) and corresponding normalized intensity profiles (e–h) of Gaussian (a,b,e,f) and vortex (c,d,g,h) components propagating separately for various input powers P_g and P_r.

To prevent the symmetry-breaking azimuthal instability of the vortex beam in the planar NLC cell we studied the interaction of two mutually incoherent two colour components— a vortex and a Gaussian beam— co-propagating in the cell as co-polarized coaxial beams. Both components were extraordinarily polarized (input E-field along the y-axis) and launched with the same Poynting directions along z. Figure 4 shows the results for two series of experiments for different input powers of the red vortex beam, namely $P_r = 5mW$ [Figs. 4(a-e)] and $P_r = 8mW$ [Figs. 4(f–j)]. These values of P_r were high enough to excite nonlinear effects and instabilities in the absence of the fundamental Gaussian beam. In both sets of experiments we kept P_r constant while we gradually changed the input power of the green beam P_g. Firstly, we monitored the power dependent dynamics of a two colour vector soliton at $P_r = 5mW$ using the red band-pass filter in front of the CCD camera in order to block the green light. For low powers of the green nematicon, $0 < P_g[mW] < 3.8$, the initially ring-shaped (red) vortex beam transformed into a dipole-like mode due to the symmetry breaking azimuthal instability, which is similar to the dipole-like vector solitons observed in other systems[37,38]. A further increase of the input power, $3.9 < P_g[mW] < 5.5$, led to a dramatic reshaping of the intensity distribution of the vortex, see Fig. 4(b). Noteworthy, at higher powers $5.6 < P_g[mW] < 8.5$ we observed a remarkable stabilization of the intensity profile of the red vortex and the formation of a vector vortex soliton which in the red component had an annular shape around a dark core, see Fig. 4(c). At higher excitations, $P_g > 8.6mW$, the spatial dynamics was amplified and the vector beam developed temporally unstable intensity distributions[39], as seen in Fig. 4(d).

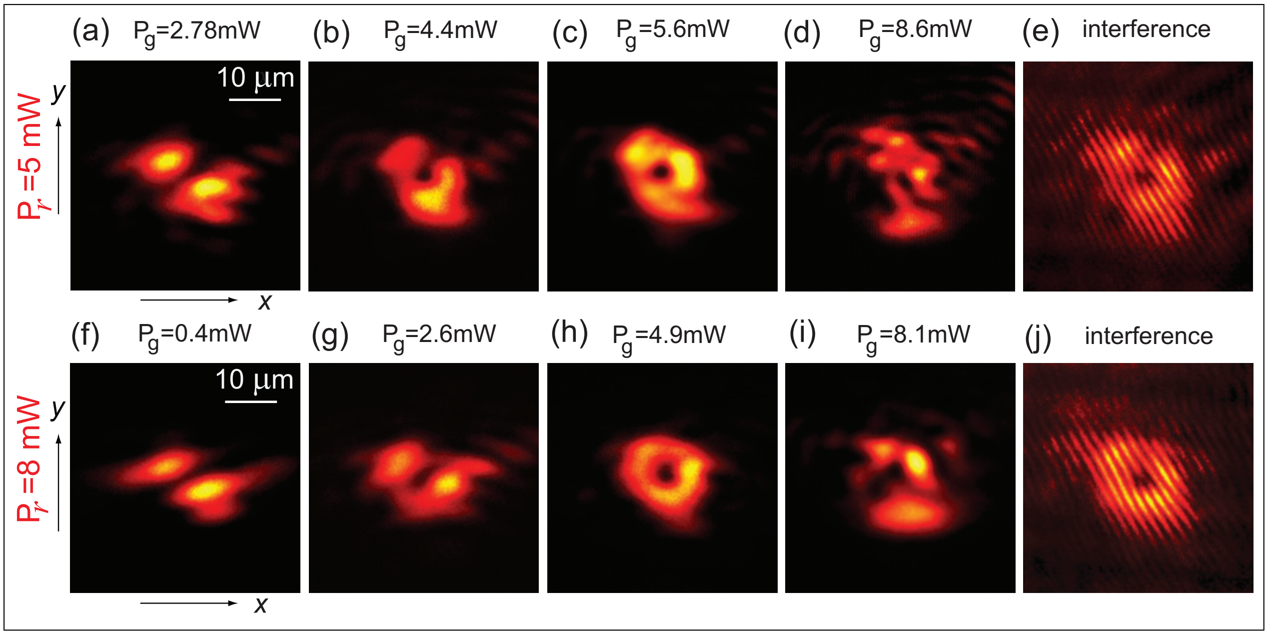

FIG. 4. (Color online) Experimental results for the output intensity distribution (a–d, f–i) and the corresponding interferograms (e,j) of the vortex (red) component of the composite vector beam for various input powers of the fundamental (Gaussian) component P_g. Images were acquired for two different input powers of the vortex (red) component $P_r = 5mW$ (a–e) and $P_r = 8mW$ (f–j)

We also observed an analogous behaviour of the vector beam at the other values of P_r. Figs. 4(f-i) present experimental results for a two-colour vector vortex beam propagating at $P_r = 8mW$ in the same NLC cell. As expected, at relatively low input powers $0 < P_g[mW] < 4.8$, the symmetry-breaking mechanism of the vortex beam leads to its azimuthal instability. However, at higher power excitations, $4.9 < P_g[mW] < 8$, the composite beam is converted into a stable circularly symmetric vector vortex soliton. Finally, as expected, for higher powers $P_g > 8.1\ mW$ we observe temporally unstable behavior. By comparing both cases for various values of the input power, i.e. $P_r = 5mW$ and $P_r = 8mW$, we observe that a stable vortex soliton can exist for a relatively broad power range which is determined by the green nematicon power and the mode mixing process.

Finally, we investigated the interferograms of the vector vortex solitons by employing a

Mach-Zehnder arrangement: a tilted broad Gaussian beam at an angle with the vector beam interferes with it at the output [see Fig. 1(c)]. The interferograms in Figs. 4(e,j) show the phase singularities by the characteristic presence of fork dislocations. Therefore, we ascertain that the vortex character of the red input beam persists after the formation of a vector soliton owing to its interaction with the nonlocal potential induced by the green nematicon. The highly nonlocal, nonlinear response of soft matter, specifically reorientational nematic liquid crystals, dramatically enhances the incoherent field coupling of two co-polarized wave-packets of different colours, leading to the stabilization of a vortex soliton when the soliton power is large enough to trap the nonlinear vortex.

III. VECTOR VORTEX-BEAM EQUATIONS

To model the experiments presented above, let us consider the propagation of two beams of polarized, coherent light of wavenumbers k_{01} and k_{02} through a cell containing undoped nematic liquid crystals. As in the experiments, the z direction is taken as the propagation direction of the beam, with the (x, y) coordinates orthogonal to this. In the absence of the optical beams the nematic molecules lie at an angle θ_0 to the z direction in the (x, z) plane. Furthermore, the molecules are constrained to rotate in the (x, z) plane under the influence of the electric fields of the optical beams. Let us denote the extra (nonlinear) rotation of the nematic molecules due to the optical beams by θ. It can be assumed that this extra rotation is small, $|\theta| \ll \theta_0$. Then in the slowly varying, paraxial approximation the equations for the electric field envelopes A_1 and A_2 of the beams and the optically induced rotation θ are[24,34,35,43]

$$\begin{aligned}
2ik_{01}n_{01}\frac{\partial A_1}{\partial z} + D_1\nabla^2 A_1 + k_{01}^2 \delta n_{a1}^2 \sin(2\theta_0) A_1 \theta = 0, \\
2ik_{02}n_{02}\frac{\partial A_2}{\partial z} + D_2\nabla^2 A_2 + k_{02}^2 \delta n_{a2}^2 \sin(2\theta_0) A_2 \theta = 0, \\
K\nabla^2\theta + \frac{1}{4}\epsilon_0 \delta n_{a1}^2 \sin(2\theta_0)|A_1|^2 + \frac{1}{4}\epsilon_0 \delta n_{a2}^2 \sin(2\theta_0)|A_2|^2 = 0,
\end{aligned} \tag{1}$$

with the Laplacian ∇^2 in the transverse (x, y) plane. The quantities n_{01} and n_{02} are the background refractive indices of the medium and δn_{a1} and δn_{a2} are the optical anisotropies at the two wavelengths, respectively[35,43]. In general, $\delta n_a^2 = n_\parallel^2 - n_\perp^2$, with $n_\parallel$ and $n_\perp$ being the refractive indices for electric fields parallel and perpendicular to the optic axis (director)

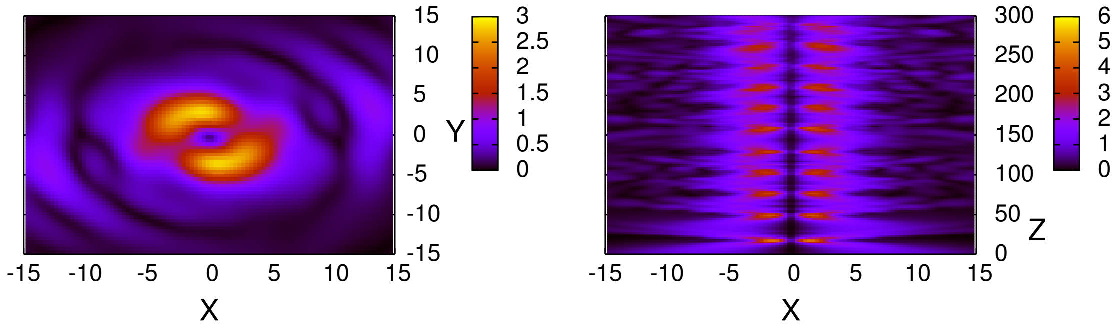

FIG. 5. (Color online) Vortex $|v|$ (a) in (X,Y) at $Z=300$ and (b) in (X,Z) without a co-propagating nematicon. The parameters for the beams are $a_u=0.0$, $a_v=0.25$ and $w_v=10.0$. The nonlocality figure is $\nu=219$.

of the NLC, respectively. In the present work the values $n_{\|}=1.67$ and $n_{\perp}=1.51$ are used, as for the nematic mixture 6CHBT at room temperature[44,45], as this is the reorientational medium used in the experiments by Izdebskaya *et al*[46]. The parameters D_1 and D_2 are the diffraction coefficients at the two wavelengths and K is the scalar elastic constant of the NLC.

The two colour nematic equations (1) can be simplified by setting them in non-dimensional form via the variable and coordinate transformations

$$X=Wx, \quad Y=Wy, \quad A_1=\alpha u, \quad A_2=\beta v, \quad Z=\gamma z. \tag{2}$$

The non-dimensional two colour nematic equations are then

$$i\frac{\partial u}{\partial Z}+\frac{1}{2}\nabla^2 u+2\theta u=0, \tag{3}$$
$$i\frac{\partial v}{\partial Z}+\frac{1}{2}D_v\nabla^2 v+2A_v\theta v=0, \tag{4}$$
$$\nu\nabla^2\theta+2|u|^2+2A_v|v|^2=0, \tag{5}$$

where the Laplacian ∇^2 is now in the transverse (X,Y) plane and the scale width W, scale amplitude β for the A_2 mode and scale propagation length γ are

$$W=\frac{2\sqrt{D_1}}{k_{01}\delta n_{a1}\sqrt{\sin(2\theta_0)}}, \quad \beta=\sqrt{\frac{k_{02}}{k_{01}}}\alpha, \quad \gamma=\frac{4n_{01}}{k_{01}\delta n_{a1}^2\sin(2\theta_0)}. \tag{6}$$

The scale amplitude α for the mode A_1 is determined from the power P_1 and width w_b of

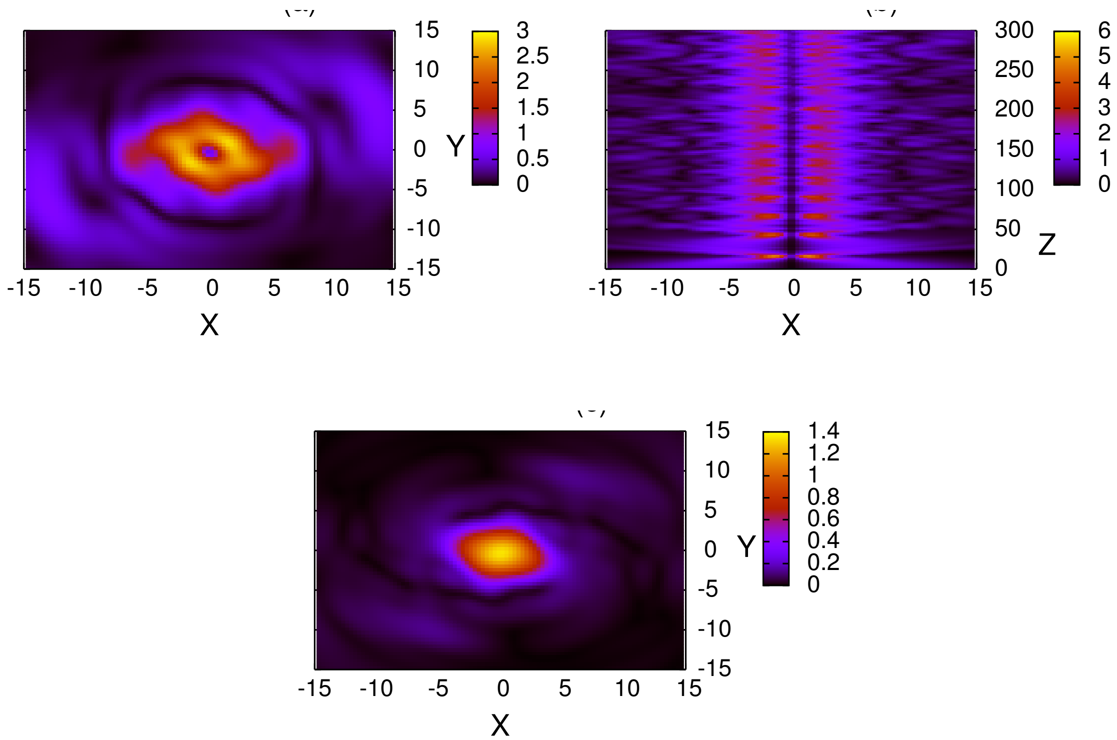

FIG. 6. (Color online) Vortex $|v|$ (a) in (X, Y)at $Z = 300$ and (b) in (X, Z) with a co-propagating nematicon. (c) Nematicon in (X, Y) at $Z = 300$. The parameters for the beams are $a_u = 0.5$, $w_u = 10$, $a_v = 0.25$ and $w_v = 10.0$. The nonlocality is $\nu = 219$.

the input beam in the A_1 mode. For a Gaussian input beam

$$P_1 = \frac{\epsilon_0}{2} c n_{01} \frac{\pi}{2} \alpha^2 w_b^2, \tag{7}$$

which determines α in terms of P_1 and w_b. The non-dimensional nonlocal response ν of the soft medium in the director equation (5) is given by

$$\nu = \frac{8K}{\epsilon_0 \delta n_{a1}^2 \alpha^2 W^2 \sin(2\theta_0)}. \tag{8}$$

Finally, the non-dimensional diffraction coefficient D_v and the coupling coefficient A_v in equation (4) for the beam v are given by

$$D_v = \frac{D_2}{D_1} \frac{k_{01} n_{01}}{k_{02} n_{02}} \quad \text{and} \quad A_v = \frac{k_{02} n_{01} \delta n_{a2}^2}{k_{01} n_{02} \delta n_{a1}^2}. \tag{9}$$

The parameter values used to non-dimensionalise the nematic equations (1) are taken from experimental data[46]. The vortex was formed from a beam at $\lambda_{02} = 671nm$ and the solitary wave at $\lambda_{01} = 532nm$, with $k_{01} = 2\pi/\lambda_{01}$ and $k_{02} = 2\pi/\lambda_{02}$. The anchoring angle was $\theta_0 = \pi/4$ in the plane (X, Z). The amplitude of the beams was scaled using (7) with the power $P_1 = 4.9mW$ and width $w_b = 4\mu m$ of the solitary wave which was found to stabilise the vortex in the experiments. Finally, the diffraction coefficients were taken to be $D_1 = D_2 = 1$ and the Frank constant $K = 1.2 \times 10^{-12}N$.

The input vortex and nematicon at $Z = 0$ are taken to have Gaussian profiles, as in the experiments, so that

$$u = a_u e^{-r^2/w_u^2}, \tag{10}$$

$$v = a_v r e^{-r^2/w_v^2} e^{i\varphi}, \tag{11}$$

where $r^2 = X^2 + Y^2$ and φ is the related polar angle.

Figure 5 shows results for an input vortex of power $10.7mW$ and radius of $2.35\mu m$ at its maximum without a co-propagating nematicon. In non-dimensional variables, $w_v = 10$ and $a_v = 0.25$. Figure 5(a) shows the vortex after it has propagated a distance $Z = 300$, i.e. the physical distance $z = 333\mu m$. It can be seen that the vortex becomes unstable due to the standard $n = 2$ symmetry breaking instability and breaks up into two beams[20]. Figure 5(b) shows the evolution of the vortex in the (X, Z) plane $(Y = 0)$. Clearly the vortex beam spreads apart as it becomes unstable, which is most apparent at the upper end of its propagation range. This is due to it breaking up into two nematicons based on the azimuthal instability.

Figure 6 shows the corresponding results when the vortex co-propagates with a nematicon of input power $0.85mW$ and Gaussian radius $3.33\mu m$, so that $w_u = 10$ and $a_u = 0.5$. The co-propagating nematicon stabilises the vortex, in agreement with the experiments[46]. Figure 6(a) shows the vortex at $Z = 300$, after propagating a physical distance of $333\mu m$, and Figure 6(c) the co-propagating nematicon after the same propagation distance. Figure 6(b) for the evolution of the vortex shows that it oscillates in amplitude and width, but holds together and does not broaden as for the isolated vortex of Figure 5(b). Note, the difference between the evolution of the unstable and stable vortices in the (X, Z) plane $(Y = 0)$ are most clearly seen around $Z = 300$ [cf. Figure 5(b) and Figure 6(b)]. The input powers for the vortex and nematicon are similar to those in the experiments, for which the input vortex had power $8mW$ and width at its maximum of $7\mu m$ and the nematicon which stabilised the vortex had a power of $4.9mW$ and a Gaussian width of $4\mu m$.

A vortex and a nematicon with the nominal powers and widths as used in the experiments (i.e. not accounting for input coupling and propagation losses) are far from steady beams for the nematicon equations (1), so they undergo large amplitude and width oscillations. The nematicon may split into two filaments[18], which is typical solitary wave behaviour for large power beams[47]; the vortex initially undergoes significant shape changes, as can be seen from Figures 5(b) and 6(b), accompanied by the shedding of diffractive radiation. This is partly due to the Gaussian profile (11) not being the exact vortex solution of the nematic equations (3)–(5), so radiation shedding moves it towards the vortex solution.

IV. CONCLUSIONS

In conclusion, we have shown experimentally and numerically that two component vector vortex solitons, for which one of the components carries an optical vortex with a single topological charge, can be stabilized using the nonlocal reorientational nonlinearity of nematic liquid crystals. We have found that the coupling with the fundamental soliton avoids astigmatic transformations of the input vortex component into spiralling dipole states that can occur in this anisotropic medium when a vortex carrying beam propagates alone. Remarkably, such composite vector solitons are observed for comparable powers of the red and green light components, indicating a strong nonlinear coupling between them. We expect that our results will further stimulate the generation of, till now, elusive types of composite solitons, such as multi-pole or multi-ring complexes and their periodic dynamical transformations and oscillations. The great potential of such controllable stable routing of vortex carrying excitations and the information encoded in their non-trivial phase distributions requires further detailed studies.

V. ACKNOWLEDGEMENTS

Y.I. and W.K. acknowledge the Australian Research Council for financial support. GA thanks the Academy of Finland for financial support through the Finland Distinguished

Professor grant no. 282858.

---

[1] J.F. Nye and M.V. Berry, Proc. R. Soc. London A **336**, 165 (1974).

[2] M.S. Soskin and M.V. Vasnetsov, Prog. Opt. **42** 219 (Ed. E. Wolf, Elsevier, 2001).

[3] A.M. Yao and M.J. Padgett, Adv. Opt. Photonics, **3**, 161 (2011).

[4] G. A. Swartzlander, *Optical vortices* (CRC Press, 2014).

[5] D.G. Grier, Nature **424**, 810 (2003).

[6] M.J. Padgett and R. Bowman, Nature Photon. **5**, 343 (2011).

[7] V.G. Shvedov, A.V. Rode, Y.V. Izdebskaya, A.S. Desyatnikov, W. Krolikowski and Y.S. Kivshar, Phys. Rev. Lett. **105**, 118103 (2010).

[8] V.G. Shvedov, A.S. Desyatnikov, A.V. Rode, Y.V. Izdebskaya, W. Krolikowski and Yu.S. Kivshar, Appl. Phys. A **100**, 2, 327 (2010).

[9] V.G. Shvedov, A.V. Rode, Y.V. Izdebskaya, D. Leykam, A.S. Desyatnikov, W. Krolikowski and Yu.S. Kivshar, J. Opt. **12**, 12, 124003 (2010).

[10] E. Brasselet and C. Loussert, Opt. Lett. **36**, 719 (2011).

[11] R. Barboza, U. Bortolozzo, G. Assanto, E. Vidal-Henriquez, M. G. Clerc, and S. Residori, Phys. Rev. Lett. **109**, 143901 (2012).

[12] E. Brasselet, Phys. Rev. Lett. **108**, 087801 (2012).

[13] R. Barboza, U. Bortolozzo, G. Assanto, E. Vidal-Henriquez, M. G. Clerc, and S. Residori, Phys. Rev. Lett. **111**, 093902 (2013).

[14] J. Wang, J-Y. Yang, I.M. Fazal, N. Ahmed, Y. Yan, H. Huang, Y. Ren, Y. Yue, S. Dolinar, M. Tur and A.E. Willner, Nature Photon. **6**, 488 (2012).

[15] G.A. Swartzlander, J. Opt. A: Pure Appl. Opt. **11**, 094022 (2009).

[16] M.R. Dennis and J.B. Götte, Phys. Rev. Lett. **109**, 183903 (2012).

[17] Y. Izdebskaya, V. Shvedov and A. Volyar, Opt. Lett. **30**, 19 (2005).

[18] Yu.S. Kivshar and G.P. Agrawal, *Optical Solitons: From Fibers to Photonic Crystals* (Acad. Press, 2003).

[19] A. Alberucci, C. P. Jisha, N. F. Smyth and G. Assanto,Phys. Rev. A **91**, 013841 (2015).

[20] A.I. Yakimenko, Yu.A. Zaliznyak and Yu.S. Kivshar, Phys. Rev. E **71**, 065603(R) (2005).

[21] D. Briedis, D.E. Petersen, D. Edmundson, W. Krolikowski and O. Bang, Opt. Express **13**, 435 (2005).

[22] C. Rotschild, O. Cohen, O. Manela, M. Segev and T. Carmon, Phys. Rev. Lett. **95**, 213904 (2005).

[23] G. Assanto, A.A. Minzoni and N.F. Smyth, Opt. Lett. **39**, 509 (2014).

[24] A. Alberucci, M. Peccianti, G. Assanto, A. Dyadyusha and M. Kaczmarek, Phys. Rev. Lett. **97,** 153903 (2006).

[25] B.D. Skuse and N.F. Smyth, Phys. Rev. A **79**, 063806 (2009).

[26] A. Fratalocchi, A. Piccardi, M. Peccianti and G. Assanto, Opt. Lett. **32**, 1447 (2007).

[27] A. Fratalocchi, A. Piccardi, M. Peccianti and G. Assanto, Phys. Rev. A **75**, 063835 (2007).

[28] G. Assanto, N.F. Smyth and A.L. Worthy, Phys. Rev. A **78**, 013832 (2008).

[29] Y.V. Izdebskaya, A.S. Desyatnikov, G. Assanto, and Yu.S. Kivshar, Opt. Express **19**, 21457 (2011).

[30] Z. Xu, Y.V. Kartashov and L. Torner, Phys. Rev. E **73**, 055601(R) (2006).

[31] Y.V. Kartashov, L. Torner, V. A. Vysloukh and D. Mihalache, Opt. Lett. **31**, 1483 (2006).

[32] Y.V. Izdebskaya, J. Rebling, A.S. Desyatnikov and Yu.S. Kivshar, Opt. Express **37**, 767 (2012).

[33] Z. Xu, N.F. Smyth, A.A. Minzoni and Y.S. Kivshar, Opt. Lett. **34**, 1414 (2009).

[34] C. Conti, M. Peccianti and G. Assanto, Phys. Rev. Lett. **91**, 073901 (2003).

[35] M. Peccianti and G. Assanto, Phys. Rep. **516**, 147 (2012).

[36] A.A. Minzoni, N.F. Smyth, Z. Xu and Y.S. Kivshar, Phys. Rev. A **79**, 063808 (2009).

[37] W. Krolikowski, E.A. Ostrovskaya, C. Weilnau, M. Geisser, G. McCarthy, Y.S. Kivshar, C. Denz and B. Luther-Davies, Phys. Rev. Lett. **85**, 1424 (2000).

[38] Y. Zhang, Z. Wang, Z. Nie, C. Li, H. Chen, K. Lu and M. Xiao, Phys. Rev. Lett. **106**, 093904 (2011).

[39] Y. Izdebskaya, A.S. Desyatnikov, G. Assanto, and Yu.S. Kivshar, Opt. Lett. **36**, 184 (2011).

[40] G. Assanto and N.F. Smyth, J. Lasers, Opt. & Photon. **1**, 1000105: 105 (2014).

[41] G. Assanto, A.A. Minzoni and N.F. Smyth, Phys. Rev. A **89**, 013827 (2014).

[42] G. Assanto and N. F. Smyth, IEEE J. Sel. Top. Quantum Electron. , 22, 4400306 (2016).

[43] G. Assanto, *Nematicons, Spatial Optical Solitons in Nematic Liquid Crystals,* John Wiley and Sons, New York (2012).

[44] M. Peccianti, A. Fratalocchi and G. Assanto, Opt. Express **12**, 6524 (2004).

[45] *CRC Handbook of Laser Science and Technology: Optical Materials*, Suppl. 2, ed. M.J. Weber, CRC Press, New York (1995).

[46] Y. Izdebskaya, G. Assanto and W. Krolikowski, Opt. Lett. **40**, 4182 (2015).

[47] E. Braun, L.P. Faucheux, and A. Libchaber, Phys. Rev. A **48**, 611 (1993).